Journal of Energy Storage 95 (2024) 112483

Contents lists available at ScienceDirect

Journal of Energy Storage

journal homepage: www.elsevier.com/locate/est

Research Papers

# Influence of inhomogeneous state of charge distributions on thermal runaway propagation in lithium-ion batteries

Michael Theiler *, Alexander Baumann, Christian Endisch

*Technische Hochschule Ingolstadt, Esplanade 10, 85049 Ingolstadt, Germany*

ARTICLE INFO

*Keywords:*
Lithium-ion battery safety
Thermal runaway
Thermal propagation
State of charge
State of charge distribution

ABSTRACT

It is well known that lithium-ion batteries pose a certain safety risk. The thermal runaway of a cell and the subsequent thermal propagation through the battery are considered particularly dangerous. Effective solutions for their mitigation are therefore of great interest. Previous studies have shown the significant influence of a cell's state of charge (SOC) on its behavior during thermal runaway. This relation may be exploitable in a battery pack to improve its safety. This study aims to assess the leverage of active SOC reduction in the imminent threat of thermal runaway. Implementing such a technique could become feasible with the emergence of reconfigurable battery systems. Four experiments were conducted, each with a module of three fresh 63 Ah high energy pouch cells in a spring-loaded bracing. The experiments studied different stationary SOC configurations, uniform (100 % and 60 %) and non-uniform (100 %–60 %–100 % and 100 %–20 %–100 %). The results indicate that thermal propagation is substantially delay (87 s) by discharging a cell in its path. The SOC reduction primarily decreases the maximum temperature of the respective cell. Further effects are a calmer thermal runaway and prolonged propagation time within the cell as well as to the next cell. In comparison, the SOC reduction has little impact on the cell's own triggering time, as the triggering time is mainly determined by the thermal energy transferred from the preceding cell and hence by its SOC. Furthermore, the analysis of the experimental data (temperature, voltage, pressure, video) gives insights into the propagation of thermal runaway through the individual layers of a cell. With reference to the position of a cell relative to the origin of the thermal propagation, a decrease of its mass loss and an increase of its internal propagation time is observed. This effect is attributed to the decreasing module pressure due to progressive loss of material. The assessment shows that active SOC reduction techniques have great leverage for mitigating or even stopping thermal propagation in a battery pack.

## 1. Introduction

Lithium-ion batteries are used in a wide range of applications but can pose a considerable potential hazard. When a cell transitions into a thermal runaway, exothermic chemical reactions and internal short circuits lead to a self-reinforcing and uncontrollable temperature increase within the cell [1]. This, in turn, can pose a considerable risk to the surrounding environment due to the intense generation of gas and flames, accompanied by high temperatures [2].

In cell modules, this results in thermal propagation when the neighboring cells are exposed to high temperatures for a sufficiently long period, causing them to enter thermal runaway. This sequence of events can lead to a chain reaction, progressively causing all cells in a battery system to undergo thermal runaway [3].

In conventional battery systems, attempts are normally made to prevent or mitigate thermal propagation by using interlayers between cells with low thermal conductivity [4] such as ceramic fiber barriers [5] or aerogel [6,7], leaving a spacing between adjacent cells [5,8] and cooling the battery actively [6,7]. Furthermore, the thermal propagation behavior also depends on the position of the first triggered cell [9], the electrical connection between cells [10–12] and the triggering method [13]. However, suppose a fault occurs during the operation of the battery system, for example in an electric vehicle, active intervention is only possible with the help of cooling. All other factors influencing thermal propagation mentioned depend on the unknown fault scenario or cannot be changed during operation.

In addition to the options already mentioned, there is another way to actively change the behavior of the thermal runaway and thermal propagation during operation. By charging or discharging the cell's state of charge (SOC) and thus the stored energy can be changed. Liu et al. [14] showed an increasing onset temperature from 198 °C at

* Corresponding author.
*E-mail address:* michael.theiler@thi.de (M. Theiler).

https://doi.org/10.1016/j.est.2024.112483
Received 25 March 2024; Received in revised form 13 May 2024; Accepted 3 June 2024
Available online 14 June 2024

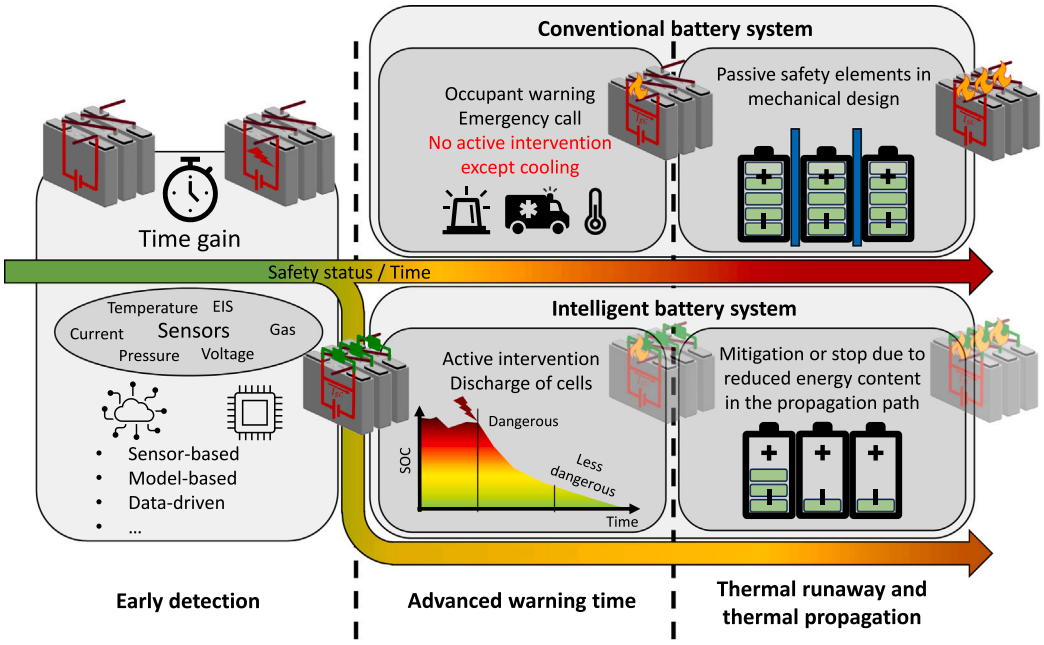


**Fig. 1.** Comparison of thermal runaway mitigation strategies between conventional battery systems with passive safety measures and intelligent battery systems with active safety measures. It is assumed that both types have systems for early fault detection in operation.

100% to 231 °C at 20% SOC and that no thermal runaway took place with 0% SOC for cylindrical 18 650 $LiCoO_2$ cells. Willstrand et al. [15] found that the generated gas volume, gas generation rate, mass loss and maximal temperature increase while the thermal runaway onset decreases with higher SOC under different abuse conditions. Furthermore, the maximal temperature depends on the mass loss since energy is lost to the environment [14,15]. The gas composition is different for various SOCs i.e. the $CO_2$ proportion declines and the CO proportion increases with SOC [15,16]. He et al. [17] modeled the chemical reactions of thermal runaway of an NMC532 cell using the Arrhenius law and measurements from differential scanning calorimetry. The model shows a SOC dependence of the onset temperature and the reaction enthalpy of the cathode–anode and anode-electrolyte reactions. With higher SOC more intercalated lithium within the anode is available for reactions with the electrolyte [16,18] and the delithiated cathode is less thermally stable and releases more oxygen, which reacts with the electrolyte [16,19,20].

By reducing the SOC of a cell undergoing thermal runaway, the released thermal energy can be reduced [4,15,17,21], which is the key to effectively delay or prevent thermal propagation according to Jin et al. [22]. Li et al. [23] found that the propagation time from cell to cell in a module increases by a factor of 3.53 and the propagation time within a cell by 3.9 when the SOC is reduced from 100% to 50%. Liu et al. [24] demonstrated for modules consisting of cylindrical 18 650 cells with 30% and 100% SOC, that the maximum cell temperature, the propagation speed, and the mass loss depend on SOC and also on ambient pressure. In [25], two stacked 18 650 cells only propagate if the SOC is higher than 50%, moreover, propagation can be prevented at higher SOCs by providing sufficient spacing between the cells. In the work of Zhu et al. [26], no propagation occurs within a module with 0% SOC, while a module with 50% SOC takes longer than one with 100% to fully undergo thermal propagation. Here again, propagation can be slowed by increasing the distance between cells. Wu et al. [27] showed that higher SOCs make it more difficult to prevent thermal propagation with the help of cooling. All the literature mentioned above used modules with homogeneous SOC distribution. Therefore, Ying et al. [28] go a step further and simulate the influence of a non-uniform SOC distribution for a module consisting of four cylindrical cells. While with a SOC distribution of 100%–70%–60%–100%, the entire module undergoes thermal propagation, in the case of a SOC distribution of 100%–30%–0%–100%, only the first two cells go into thermal runaway.

The literature review confirms the assumption that, SOC significantly influences thermal runaway at the cell level and thermal propagation at the module level. This relation might be exploitable which opens up new possibilities for reacting to imminent battery system faults. This is illustrated in Fig. 1 by comparing a conventional battery system (upper time line) with an intelligent reconfigurable battery system (lower time line). During normal operation, both battery systems attempt to detect potential faults as early as possible through various sensors and methods as reviewed for example in [29–31]. If a fault is detected, the conventional system cannot actively influence the system beyond ramping up the cooling system, and their response is limited to warning the surrounding area and alerting the emergency services. Subsequently, only the known passive safety elements and cooling can prevent or delay thermal propagation [32–34]. Reducing the SOC is generally not feasible for conventional systems, as all cells have to be discharged simultaneously and therefore a large amount of energy has to be discharged in a short time.

In contrast, intelligent reconfigurable battery systems, as highlighted and reviewed by Komsiyska et al. [35], offer the distinct advantage of selectively discharging individual cells or specific modules using switches. It allows, to use the available time period between error detection and thermal runaway not only for cooling but also to reduce the SOC of individual cells, as proposed by Ying et al. [28] and Feng et al. [36]. This ability may reduce the risk and probability of thermal runaway for individual cells as well as mitigate or even stop thermal propagation. The implementation of this operational strategy could lead to reduced requirements for additional safety systems, such as oversized cooling or thermal insulators between cells in the battery system [25,27] and can therefore avoid over-designed safety measures for extreme error scenarios. To thoroughly assess and analyze the implications of the aforementioned safety strategy, it is necessary to gain a comprehensive understanding of the influence of the SOC distribution on thermal propagation, especially in the case of inhomogeneous distributions.

To the best of the author's knowledge, there are no published experiments on the influence of inhomogeneous SOC distributions on

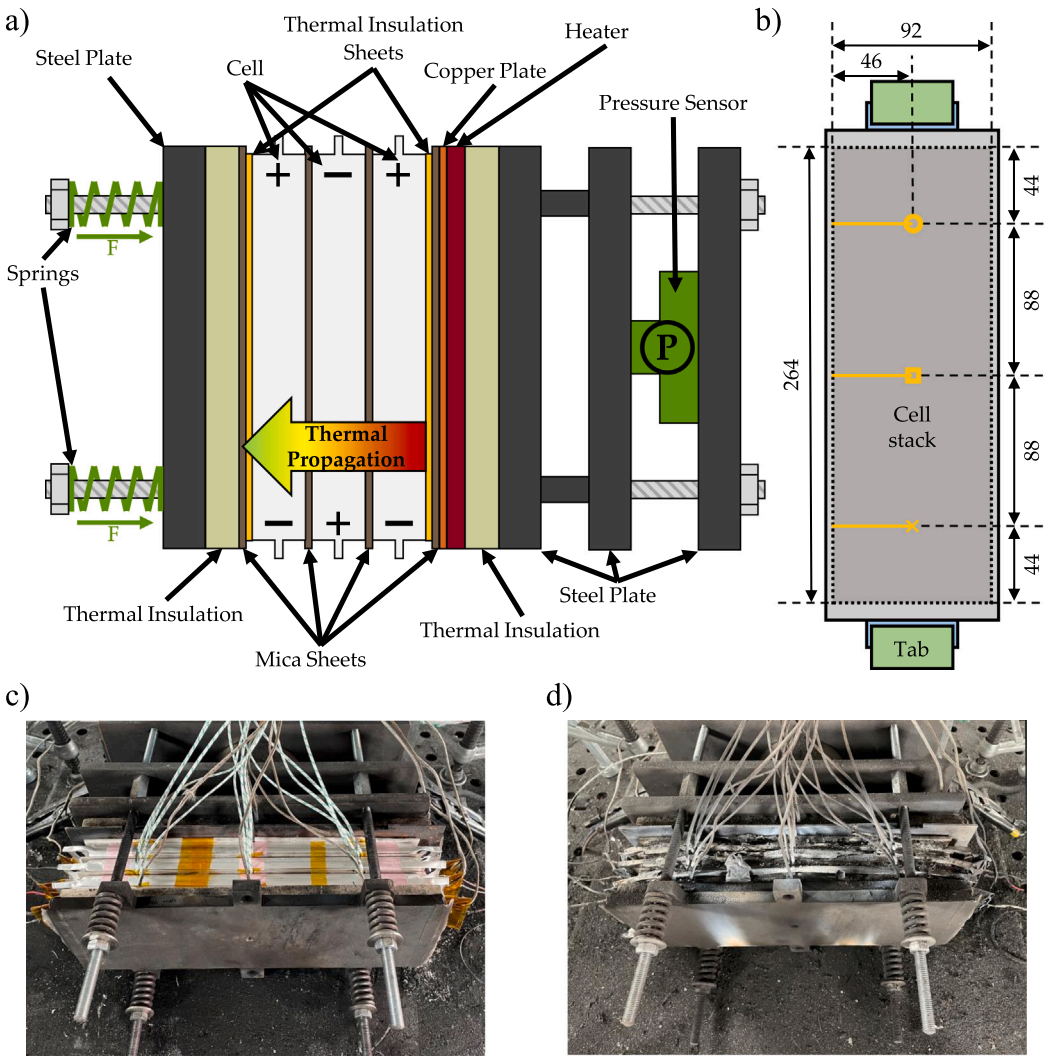


**Fig. 2.** Illustration of the experimental setup including (a) the module and the bracing, (b) the cell size (Lengths are given in millimeter) and thermocouple positioning, (c) picture before and (d) picture after an experiment. (For interpretation of the references to color in this figure legend, the reader is referred to the web version of this article.)

thermal propagation, especially for high-energy pouch cell modules. With this publication, we try to close that research gap. Intelligent battery systems are an up-and-coming topic in energy storage research and they may become relevant for battery manufacturers in the near future. Active safety measures have great potential to play a large role in making intelligent battery systems economically feasible.

The remainder of this contribution is structured as follows: Section 2 explains the experimental setup including the cell, the module bracing, the sensors and the conducted experiments. In Section 3 the data processing is described before in the following Section 4 the results are shown and discussed. This includes the evaluation of some thermal propagation characteristics like maximal cell temperatures, propagation time and mass loss as well as in-depth video analysis.

**Table 1**
Specification of the lithium-ion cell used in the experiments.

| Format | Pouch | Unit |
|---|---|---|
| Chemistry | NMC | |
| Nominal capacity | 63 | Ah |
| Charge cut-off-voltage | 4.25 | V |
| Discharge cut-off-voltage | 2.75 | V |
| Maximum continuous charge current rate | 1C | |
| Maximum continuous discharge current rate | 3C | |
| Nominal voltage | 3.7 | V |
| Weight | 866 | g |
| Gravimetric energy density | 269 | Wh/kg |
| Cell tabs | Opposing | |
| Cellstack size | 264 × 92 × 14 | mm |

## 2. Experimental setup

The cell under study is a 63 Ah high-energy pouch cell with opposing tabs. It has a graphite anode and an NMC (LiNiMnCoO2) type cathode material with the specifications given in Table 1 according to the cell distributor and own measurements. Based on preliminary tests, it is assumed that the cell has a ceramic-coated separator, as the cell only showed signs of internal short circuits at temperatures well above 165 °C [37].

Before installing the cells into modules, all cells were preconditioned with at least two cycles consisting of a C/2 constant-current discharge and a C/2 constant-current charge until the charge cut-off-voltage was reached followed by a constant-voltage phase until the current dropped below C/20.

The experimental setup for all thermal propagation experiments is shown in Fig. 2. The module in Fig. 2a consists of three cells separated by an intermediate layer of 1 mm thick mica plates. On both sides of the module, there were also 1 mm thick mica plates and heat insulating sheets of calcium magnesium silicate, which provide a flat, uniform and heat insulated bracing. Each mica plate had three cuts

**Table 2**
SOC distributions within the modules during the four experiments conducted.

| SOC cell 1 [%] | SOC cell 2 [%] | SOC cell 3 [%] | Propagation time [s] |
|---|---|---|---|
| 100 | 100 | 100 | 83 |
| 100 | 60 | 100 | 98 |
| 60 | 60 | 60 | 122 |
| 100 | 20 | 100 | 170 |

on the long cell side, such that three type-K thermocouples GG-KI-30-SLE from Omega could be placed on the surface of both cell sides to measure possible uneven surface temperature as recommended by [38]. The thermocouple measurement positioning is depicted by the yellow markers and the thermocouple cable is represented by the yellow lines in Fig. 2b. The markers are used in the temperature plots to distinguish the different temperature measurement points on the same cell surface. The cells were not electrically connected, as heat transfer between pouch cells is dominated by the cell surface and not by the tabs [10,39].

To trigger the first cell of the module a 1.6 kW heating plate was placed on one side of the module. Between the first cell and the heating plate, a 2 mm copper plate was inserted to ensure an even heat distribution since a thermal video and previously conducted experiments showed uneven heating of the heating plate. The heating plate was controlled with the maximum power, since a high heating power introduces the least heat flux energy to trigger the first cell and thus has the least effect on the thermal propagation process [22]. Therefore, this prevents the temperature of the middle and last cell from rising significantly before the first cell goes into thermal runaway. The heater was automatically switched off, when the measured temperature on the heated cell side reached 350 °C.

The entire structure was braced with 10 mm thick thermal insulation layers and 10 mm steel plates. Four springs were used to adjust the module pressure evenly to around 80 kPa, which is in the order of magnitude of values provided by cell manufacturers [40]. Each spring has a total length of 35 mm and a stiffness of 171.72 N/mm. The pressure of the whole module was measured with a load cell. To protect the load cell from high temperatures and flames, another steel plate was installed between the module and the load cell. Pictures before and after an experiment are provided in Fig. 2c and d.

Measurements were acquired using the NI cDAQ-9178 chassis. The temperature data was measured via NI 9213 with a sampling rate of 75 Hz and the cell voltages as well as the output pressure signal of the load cell were measured via the NI 9239 with 2 kHz. Video recordings were made with a GoPro Hero 8 camera with 120 frames per second (fps).

A total of four module experiments were conducted with different SOC distributions. The SOC specifications for these tests are indicated in Table 2. Experiment 1 and 3 maintain a homogeneous SOC distribution with 100% and 60% SOC, to display the influence of SOC on thermal propagation and to serve as reference tests for comparison. The remaining two tests feature an inhomogeneous SOC distribution. In these tests, the first and the last cell consistently have a SOC of 100%, while the second cell has a SOC of 60% and 20%, respectively.

## 3. Data processing

The measurement data were filtered and cleaned of outliers before analysis, which were generated, for example, by an electrical contact of the thermocouples with the cell due to severe rupture of the cell and melting of the cell housing. Fig. 3a–d show all relevant cell surface temperatures and voltages over a period of 200 s from the first trigger time onwards for the corresponding experiments.

The trigger time for each individual temperature sensor, marked by red shapes, were chosen based on the rate of temperature rise threshold of 50 K/s. The threshold value itself was chosen because it determines the trigger time well and robustly in the case of the measured data without any significant delay. In all experiments, the front surface of cell 2 and 3 show two significant temperature increases. One due to the heat release of the previous cell and one due to the heat release of the cell itself. Therefore, time ranges in which the previous cell could cause a temperature rise of more than 50 K/s were not taken into account. An exception is the front of cell 2 in the 100%–20%–100% test. Since the heating rate is too low, the trigger time was determined manually based on the temperature curve and the video material.

In Fig. 3a–d the solid lines represent the temperature sensors on the front cell side facing the heating plate and the dashed lines represent the opposite side averting the heating plate. The different markers correspond to the respective thermocouple positions on the cell surface in Fig. 2b. It should be noted that the marker positions are independent of the cell polarity, such that the thermocouples with the same marker are on the same side of the module.

In the 100%–100%–100% test, there is an influence on some temperature sensors at about 10 s in Fig. 3a, probably due to the flames and the thermal runaway of the first cell. This leads to implausible temperature readings for the back surface of cell 2 and for both cell sides of cell 3. This time range was also disregarded for the corresponding sensors.

Therefore, a total of three thermocouples are on each cell surface and thus three trigger times $t^f_{i,n}$ can be determined for the front and also three trigger times $t^b_{i,n}$ for the back of the respective cell $i$. For further evaluation the average trigger times $\overline{t^f_i}$ and $\overline{t^b_i}$ are calculated according to

$$\overline{t^f_i} = \frac{1}{N}\sum_{n=1}^{N} t^f_{i,n} \tag{1}$$

$$\overline{t^b_i} = \frac{1}{N}\sum_{n=1}^{N} t^b_{i,n} \tag{2}$$

with $1 \leq n \leq N$, $N = 3$ and $i \in \{1, 2, 3\}$.

The voltage data presented is also subject to filtering and in the event that the voltage drops below 10 mV or fluctuates around 0 V after a thermal runaway for a significant period of time, the voltage value is set to 0 V.

The module pressure recorded via the load cell is filtered and shown also for 200 s beginning with the first trigger time in each respective experiment in Fig. 3e. It is noteworthy that the pressure value at the beginning of the displayed duration can deviate from the initial pressure, as the venting of the cell and some chemical reaction have already occurred and the temperature of the cell stack is elevated.

Due to the absence of recorded mass data for some individual cells prior to testing, the mean value derived from multiple intact cells is utilized as the mass for each cell before the experiments. This averaged mass is the value given in Table 1.

## 4. Results and discussions

When comparing the overall duration of the modules' thermal propagation in the experiments according to Table 2, from the first trigger time in cell 1 to the last trigger time in cell 3, a clear dependency on the distribution of the SOC becomes apparent. Simply by changing the SOC of cell 2 from 100% to 20%, the propagation time can be significantly prolonged by 87 s (factor of 2). In comparison to the homogeneous 60% SOC test the propagation was still delayed by 48 s. This alone illustrates the potential for reducing the SOC through a discharge strategy in the event of a fault. To gain a better understanding of the propagation duration and its influencing factors, various features of thermal propagation are analyzed below. This includes the propagation time from one cell to the next cell $\Delta t_{(i-1)\rightarrow i}$, the propagation time from the front of the cell to the back $\Delta t_i$ and the maximum cell temperatures $T_{\max}$ similar as in [23]. Furthermore, the mass loss of each cell and video footage are evaluated.

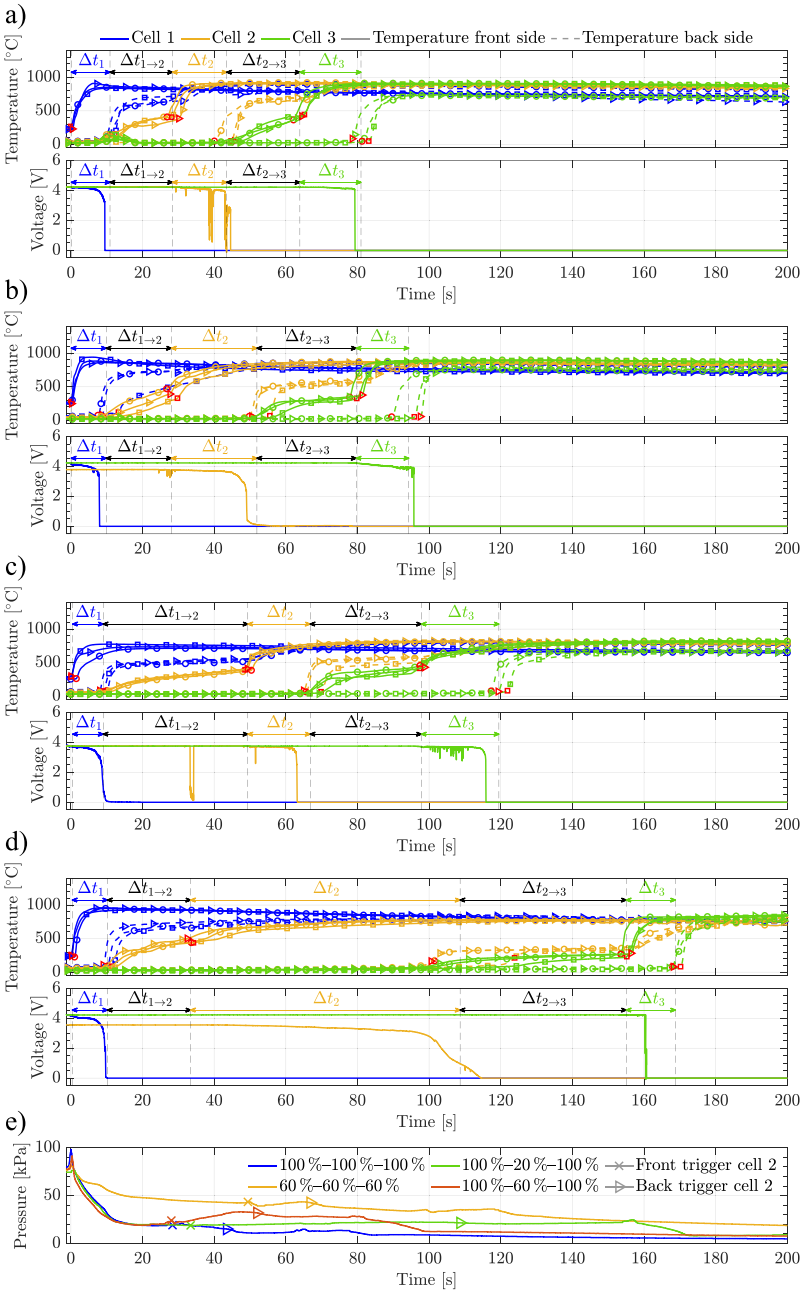


**Fig. 3.** The diagrams show the temperature and voltage data for the (a) 100%–100%–100%, (b) 100%–60%–100%, (c) 60%–60%–60% and (d) 100%–20%–100% SOC experiment. In the temperature diagram, the temperatures measured at the front of the cell are shown with a solid line and the temperatures measured at the back of the cell are shown with a dashed line. The module pressure is shown for all tests in (e) including the trigger times for the second cell. (For interpretation of the references to color in this figure legend, the reader is referred to the web version of this article.)

**Table 3**
Average maximum cell back surface temperature for each SOC across all cells and experiments.

| SOC [%] | 100 | 60 | 20 |
|---|---|---|---|
| $T_{max}$ [°C] | 709 | 584 | 350 |

### 4.1. Maximum temperature

The SOC dependency is made clear by observing the maximum cell temperature occurring during thermal runaway. In this study, the maximum cell temperature of cell $i$ is defined as the maximum temperature on the back side of the cell as this surface temperature serves as a measure of the released energy and the intensity of the cell reactions during thermal runaway, as well as the potential harm for the next adjacent cell $i+1$. Because this temperature can be strongly affected by the thermal runaway of the next cell, only measurements taken before the next cell $i+1$ enters thermal runaway are considered. The resulting values are depicted in Fig. 4a over the cell position $i$.

When examining the maximum temperatures at the back of the cells in experiment 1 and 3 with homogeneous SOC distribution (shown in blue and orange), a temperature increase is observed with increasing cell position. This can be explained by the fact that as thermal propagation progresses, the stored thermal energy within the experimental setup and thus the average module temperature increases. Furthermore, the thermal connection between cells might decrease due to decreasing pressure, as shown in Fig. 3e, but also because cells that have previously experienced thermal runaway can no longer be considered pure solids

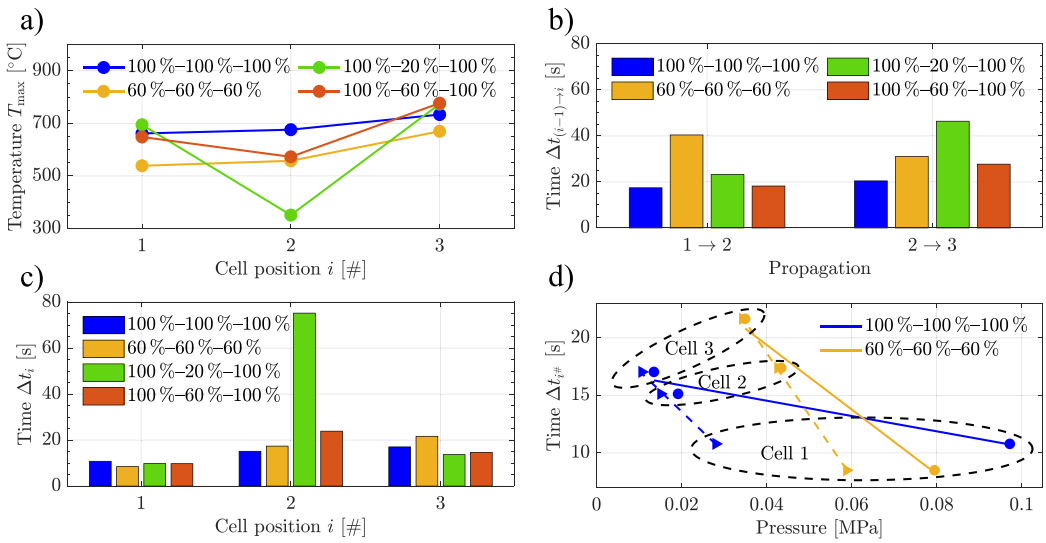


**Fig. 4.** Comparison of all four module experiments in terms of (a) the maximum temperature of the back surface of the cell $T_{max}$, (b) the propagation time from cell to cell $\Delta t_{(i-1)\to i}$, (c) the propagation time from the front surface of the cell to the back surface $\Delta t_i$ and (d) the pressure dependency of the cell internal propagation time. In (d) circle markers with the fitted solid line represent the internal propagation time in dependence on the measured pressure at the average trigger time of the cell front, while triangle markers with the fitted dashed line represent this in dependence on the measured pressure at the average trigger time of the cell back. (For interpretation of the references to color in this figure legend, the reader is referred to the web version of this article.)

due to mass ejection [41,42]. Due to its good thermal insulation on the back, the last cell releases comparatively less heat energy to the environment. In the event of a thermal runaway, this ensures that more thermal energy remains within the cell itself. Furthermore, using the average values of the maximum cell back side temperature for each SOC across all cells from the four module experiments, Table 3 shows that the SOC has a significant influence on the maximum temperature caused during thermal runaway. The maximum temperature decreases by 358.1 °C and therefore by more than 50% when the SOC decreases from 100% to 20%. In summary, reduced SOC results in less intense thermal runaway with lower temperatures and increased safety.

### 4.2. Propagation time between cells

The propagation time between cells in a module is calculated by the difference of the average trigger time on the front of the cell $i$ $\overline{t_i^f}$ and the average trigger time on the back of the preceding cell $i-1$ $\overline{t_{i-1}^b}$. The resulting time duration $\Delta t_{(i-1)\to i}$ is indicated for each experiment in the corresponding diagram in Fig. 3a–d.

Fig. 4b shows this time duration for the propagation of cell 1 to cell 2 and of cell 2 to cell 3 for all conducted experiments. It illustrates that the SOC of cell $i-1$ and the resulting heat output has a big influence on the propagation time from cell $i-1$ to cell $i$. In the experiment with an even SOC distribution of 60%, the propagation time from cell 1 to cell 2 is noticeably at least 17 s longer than in all other module tests. Also, a lower SOC of the cell $i$ seems to have a positive effect. However, the associated influence is less than that of cell $i-1$ since reducing the SOC from 100% to 60% or 20% in cell 2 only leads to a delay in the propagation from cell 1 to cell 2 of 0.77 s or 5.79 s, respectively. The same tendency can be observed for the propagation time from cell 2 to 3. In the experiments with a SOC of 100% of the last cell 3, the propagation time is extended by 7.27 s or 25.93 s, if cell 2 has 60% or 20% instead of 100% SOC. In contrast, the additional reduction in cell 3's SOC to 60% in the experiment with a SOC distribution of 60%–60%–60% only has an advantage of 3.33 s over the 100%–60%–100% test.

While single-cell experiments in the literature show a strong SOC dependency of the onset temperature of the thermal runaway [15], this effect does not seem to have a major influence on thermal propagation and its speed. However, the propagation time is significantly influenced by the reduction in thermal energy released by the previous cell and thus by the SOC of the cell $i-1$.

### 4.3. Propagation time within cells

When cells are one-sided heated as in these module experiments, thermal runaway is initiated close to the heated side and subsequently spreads throughout the entire cell [23,43] leading to a high difference between the back and front temperature as can be seen in Fig. 3a–d. The propagation time required to transfer heat from the front to the back of a cell provides a quantitative measure for the speed and uniformity of the propagation within the cell as well as for the intensity of the thermal runaway [23].

In this work, this internal propagation time $\Delta t_i$ is defined, as shown in Fig. 3a–d, as the time period between the average trigger time on the back of the cell $i$ $\overline{t_i^b}$ and the average trigger time on the front $\overline{t_i^f}$ of the same cell. Fig. 4c compares this time duration for all cells across position $i$ in the experiments performed.

It becomes evident that the propagation time within a cell in experiments with a homogeneous distribution of the SOC (represented in blue and orange) increases with rising cell position $i$. To explain this Fig. 4d provides a closer examination of the relationship between module pressure and propagation time within a cell. Circle markers with the fitted solid line represent the internal propagation time in dependence on the measured pressure at the average trigger time on the cell front $\overline{t_i^f}$, while triangle markers with the fitted dashed line represent this in dependence on the measured pressure at the average trigger time on the cell back $\overline{t_i^b}$. As also visible in Fig. 3e at the start of the thermal runaway at the front of the first cell, the module pressure is high and drops during thermal runaway since gas – abruptly formed in the cell by electrolyte evaporation and chemical reactions – and particles are released [44]. Towards the end of the thermal runaway, the housing of the pouch cell is severely deformed and is often largely melted. The resulting lower module pressure after thermal runaway leads to the individual layers in the cells of the module being less compressed, which reduces the thermal through-plane conductivity within the cell [45,46]. This is because under higher pressure, gas between the cell layers is pressed to outer areas of the pouch cell [47], and individual particles have better contact with each other [48]. Therefore, as thermal propagation progresses, the module pressure

tends to decrease, which leads to a longer internal cell propagation as shown in Fig. 4d. In addition, the pressure change between $\overline{t_i^f}$ and $\overline{t_i^b}$ decreases as the position of the cell increases, depending on the stiffness of the spring used in the experimental setup. However, as observable in Fig. 3e there are also cases, for example, cell 2 in the 100%–60%–100% SOC experiment, where the pressure may increase during the event.

When comparing the first cells in Fig. 4c, no trend among themselves is visible with an average internal propagation time of 9.71 s. Cell 1 only serves as the initiator for the thermal propagation and its behavior strongly depends on the heating process, which is why no particular attention is placed on this cell.

In contrast, the cells at position 2 show a clear trend. While the cell with a SOC of 100% requires only 15.13 s for the temperature to pass, the two cells with a SOC of 60% require on average 20.63 s and the one with 20% 75.21 s. The front of the 20% cell, as shown in Fig. 3d, initially heats up only due to the thermal runaway of the previous cell. From approximately 20 s onwards slight temperature increases due to internal reactions are visible. Nevertheless, in comparison to the other cells, the considered cell does not show a rapid temperature increase on the front. This indicates that no strong instant reactions occur homogeneously in large areas of the cell with 20% SOC.

The significantly longer propagation time for the 20% cell can be explained by the already observed lower release of heat energy. In a cell with a high SOC, larger temperature gradients in the cell occur leading to a higher heat flow and therefore to a faster propagation speed [43]. Furthermore, gas is generated inside the cell due to chemical reactions and electrolyte evaporation, separating the cell stack layers [41,49]. The separation slows the heat transfer between the layers resulting in an increased thermal resistance between cell stack and cell casing and within cell stack as modeled by Chen et al. [50]. The authors added an additional thermal resistance as soon as a critical gas formation temperature is reached. After the cell ruptures and the gas escapes, this resistance decreases but does not drop to zero [50]. In particular, the pressure profile in Fig. 3e for cell 2 in the 100%–20%–100% SOC test (green line) shows a significantly longer and continuous increase between the trigger time at the front $\overline{t_2^f}$ (× marker) and the back $\overline{t_2^b}$ (▷ marker) of the second cell. This indicates continuous gas formation within the cell. It is assumed that in the 20% cell, as shown in simplified form in Fig. 5, the chemical reactions and electrolyte evaporation on the hot side of the cell gradually generate gas. This gas can escape as soon as the pouch casing ruptures, but it still pushes the individual layers apart, reducing the thermal conductivity between them. When subsequent layers reach a certain temperature, gas also forms there lowering the thermal conductivity to the following layers. This process then moves through the different layers. Particularly in cases with low SOC, the reactions proceed more slowly, leading to gas formation over a longer period and slower thermal propagation in the cell stack. This process would also explain the enormous temperature decoupling of the front and back of the cell, which is visible in all tests.

Another important point in Fig. 4c is the 6.49 s longer internal propagation time of the second cell with a SOC of 60% in the 100%–60%–100% SOC test than in the 60%–60%–60% SOC test. A possible explanation is the temperature level of the cells and thus how evenly the temperature rises within a cell. The average back side temperature of cell 2 when the thermal runaway starts in the 100%–60%–100% experiment is 26.85 °C, which is 11.77 °C lower than in the 60%–60%–60% experiment due to the faster propagation time from cell 1 to 2 resulting from the higher SOC of cell 1. When comparing the third cells, a similar trend becomes apparent. A dependency between the internal propagation time of the third cells with 100% SOC and the SOC of cell 2 is visible. In the 100%–20%–100% experiment, the average temperature on the back side of cell 3 reaches about 51.22 °C when the thermal runaway starts on the front surface with an internal propagation time of 13.72 s. In contrast, the propagation time is higher for the 100%–60%–100% SOC (14.68 s) and 100%–100%–100% SOC (17.04 s)

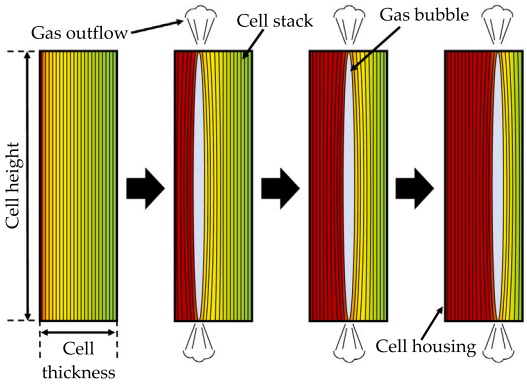


**Fig. 5.** Formation of a gas bubble as a thermal barrier between the layers of a cell, slowing the thermal propagation. (For interpretation of the references to color in this figure legend, the reader is referred to the web version of this article.)

experiment with a back side temperature of approximately 25.20 °C and 24.78 °C, respectively. These temperature differences suggest that the propagation time within a cell is influenced by the temperature level and its distribution in the cell. A SOC reduction of the previous cell leads to a lower heating rate of the following cell with a longer cell to cell propagation time as discussed earlier. This in turn results in a shorter cell internal propagation time due to the more even temperature rise within the cell. The closer the temperature level is to the thermal runaway trigger temperature, the faster the thermal propagation occurs within the cell. The observed results are in good agreement with the findings from the single-cell experiments conducted by Huang et al. [51] in which one-sided heating with heating powers between 400 W and 700 W showed that the internal propagation time increases with the heating power. Furthermore, Willstrand et al. [15] found that a cell undergoes more rapid gas formation at a comparable total gas amount when a cell is heated more evenly or slowly, as it passes through more quickly.

The last cells show a slight increase in propagation time from an average of 15.15 s for fully charged cells to 21.65 s for the cell with a SOC of 60%.

### 4.4. Mass loss

The cell mass loss is the difference between the mass of a cell before and after the experiment. As can be observed in Fig. 6a, there is a strong correlation between the mass loss and the SOC, resulting in an average mass loss of 189.6 g, 299.4 g and 409.3 g for the cells with 20%, 60% and 100% SOC, respectively. The intensity of the chemical reactions and the energy released increases with the amount of stored electrical energy, which also increases mass loss. However, the box chart clearly shows a high variation of the values for 100% and 60% SOC with a standard deviation of 19.56 g and 58.36 g, respectively. As only one cell was tested at 20%, no variation is visible for this SOC. The large differences can be explained at least in part by the cell placement or cell number $i$ within the module. The mass loss is displayed in relation to the cell number $i$ in Fig. 6b. A significant reduction of mass loss with an increase in the cell number $i$ is observed in the two tests with homogeneously distributed SOC (see the orange and blue data with the fitted line). This effect is assigned to the previously described reduction of module pressure during thermal propagation. If the cell is under preload, the individual cell stack layers are more compacted and the gas produced during thermal runaway can only escape via limited pathways from the cell [52]. This leads to the creation of local hotspots and gases, which entrain particles when they are released [52]. This relationship between mass loss and module pressure is illustrated in Fig. 6c. Circle markers with the fitted solid line represent the mass

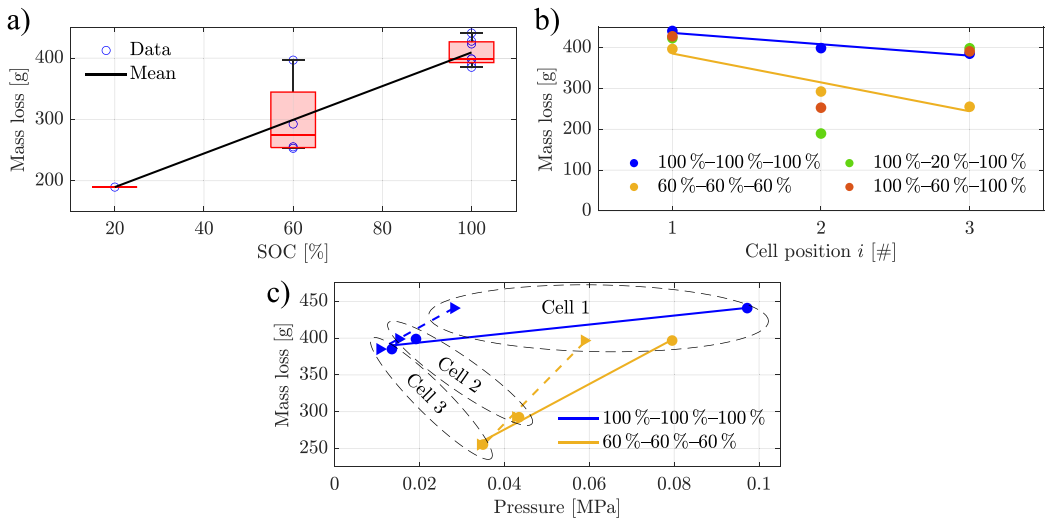


**Fig. 6.** Illustration of the dependency of the mass loss on the (a) SOC, (b) cell position and (c) measured module pressure. In (c) circle markers with the fitted solid line represent the mass loss in dependence on the measured pressure at the average trigger time of the cell front, while triangle markers with the fitted dashed line represent this in dependence on the measured pressure at the average trigger time of the cell back. (For interpretation of the references to color in this figure legend, the reader is referred to the web version of this article.)

loss dependency with the measured pressure at the average trigger time on the front of the cell, while triangle markers with the fitted dashed line represent this with measured pressure at the average trigger time on the back of the cell. For the homogeneous 60% and 100% experiments the mass loss reduces significantly from the first to the last cell by 142.55 g and 55.94 g, respectively. Therefore, the influence of the pressure seems to be more pronounced for lower SOCs. The decreasing mass loss is another reason for the increasing maximum temperature in Fig. 4a over the cell position $i$. With decreasing mass loss during the event, less energy and partially unreacted mass is released to the environment [14,15,51].

### 4.5. Comparison of the video footage for different SOCs

To illustrate the impact of SOC, this section conducts a comprehensive analysis of video recordings from the second cells in experiments with the SOC distributions of 100%–100%–100%, 100%–60%–100%, and 100%–20%–100%. The comparison involves the temperature as well as the voltage data in Fig. 3a–d and the video footage of the second cells with 100%, 60%, and 20% SOC, each triggered by the thermal runaway of the previous 100% SOC cell. Fig. 7 presents relevant frames with timestamps, utilizing distinct background colors to highlight different SOCs (blue for 100% SOC, red for 60% SOC, and orange for 20% SOC). The images capture both the initial and last trigger time for the cells, with additional time points for enhanced differentiation of cell behavior attributed to varying SOCs. Each frame includes the absolute time $t_{abs}$ concerning the module's first trigger time as in Fig. 3a–d and the relative time $t_{rel}$ to the first trigger time of the second cell.

After cell 1 has released a substantial amount of thermal energy in the 100%–100%–100% SOC experiment, the second cell with 100% SOC goes into a thermal runaway at second 27. After two more seconds, the cell shows very strong fire jets and the voltage begins to drop slightly, while the temperature rises sharply. Around 3 to 4 s later, more prominent and discernible fire jets emerge, spreading laterally from the cell in all directions. These strong fire jets last until about second 19 and become weaker when the back side enters thermal runaway. The voltage of this cell shows some drops and recoveries during the whole process due to internal short circuits and drops suddenly to 0 V 18 s after thermal runaway initiation.

The second cell in the 100%–60%–100% configuration exhibits strong fire jets after 2 s which intensify until 6 s while the temperature increases comparatively slower than the 100% SOC cell. The fire jet intensity remains constant until approximately 20 s after the first trigger time and then slowly decreases. The fire jets are still dangerous and intensive but less compared to the 100% SOC cell and last a little bit longer. Initially, the voltage fluctuates and begins to fall slowly before the voltage drops more rapidly towards 0 V around 22 s after the thermal runaway initiation. In comparison to the 100% SOC cell, the thermal runaway is less intense, prolonged and the voltage exhibits a steadier and slower decline towards 0 V.

After thermal runaway of the first cell in the 100%–20%–100% SOC experiment, cell 2 with 20% SOC begins to heat up. Initially, the fire visible is largely due to cell 1, but gradually additional flames and gas outflows become visible, like in the first image at the right side of the cell. These reach their peak after around 7 s and remain at a similar level, with stronger gas ejections and flames, as can be seen in the images at 38 s and 68 s after initiation. From approximately 75 s onwards the flame intensity decreases and after the last trigger time at about 91 s for cell 2 is reached, no additional strong flames and gas emissions occur. In contrast to the cells with higher SOCs, the process runs noticeably longer and weaker without strong fire jets, but with a continuous gas generation. Similar to the findings reported in [23], it appears that the heat and the chemical reactions within the cell stack gradually spread – beginning at the front of the cell, progressing to the back of the cell – and the speed of this process is SOC-dependent. This is indicated by the initially comparatively slow increase of the front cell temperature in Fig. 3d and the SOC-dependent propagation time $\Delta t_i$ within the cells in Fig. 4c. Furthermore, it remains unclear whether the 20% cell reaches thermal runaway or not and how much thermal energy is released in the process. The video recordings indicate that the cell material mainly burns without thermal runaway reactions. The electrolyte evaporates and begins to burn outside the cell due to the flames present. However, the electrolyte does not appear to be significantly involved in the chemical reactions within the cell. Therefore, little energy can be released by the reaction of the electrolyte with the oxygen released by the cathode, which is a major factor for thermal runaway [53]. The voltage of the 20% SOC cell, also shown in Fig. 8a, remains constant at the beginning of the temperature rise and begins to drop slightly 7 s after the first trigger time, before a stronger drop to 0 V can be observed from 63 s onwards. The voltage curve also shows that parts of the cell are still electrically intact even when the initial layers of the cell stack reach high temperature. In summary, it can be said that the intensity of the thermal runaway and the resulting flames decrease significantly with the SOC, while


**Fig. 7.** Comparison of the video footage of the second cell in the 100%–100%–100% (blue), 100%–60%–100% (red) and 100%–20%–100% (orange) experiment. (For interpretation of the references to color in this figure legend, the reader is referred to the web version of this article.)

the duration of the internal propagation increases. In addition, the measured voltage behaves differently and needs longer to drop to zero with decreasing SOC. An explanation of the voltage course especially for the 20% SOC case is given in the next subsection.

### 4.6. Detailed analysis of the 20% SOC cell's voltage

The consideration of modeling a cell stack of one cell as a parallel connection of many individual sub-cells [54,55] enables a possible explanation of the voltage course of the 20% SOC cell in Fig. 8a. Each sub-cell may have an internal short circuit over a resistance [56]. The resulting equivalent circuit model (ECM) is shown in Fig. 8b. With $N$ sub-cells and $1 \leq n \leq N$, $V_{\mathrm{OCV},n}$ represents the open circuit voltage, $R_{\mathrm{i},n}$ the internal resistance, $R_{\mathrm{isc},n}$ the internal short circuit resistance, $S_{\mathrm{isc},n}$ the internal short circuit switch and $S_{\mathrm{active},n}$ the active switch of the $n$th sub-cell.

Initially, the entire cell is intact and no internal short circuit exists. If a cell is heated on one side, short circuits may occur in sub-cells near the heated side. Therefore, $S_{\mathrm{isc},n}$ closes for these sub-cells. However, the total cell voltage does not drop rapidly, as the other intact sub-cells support the voltage of the short-circuited sub-cell utilizing a current flow [57]. After a thermal runaway or reaching high temperature, a sub-cell may no longer be electrically intact or may become disconnected from the cell stack [58]. In the context of the ECM, this means an opening of the corresponding $S_{\mathrm{active},n}$. As a result, the SOC and thus the voltage decrease depending on the current flow. The current flow in the individual sub-cells depends on the short circuit resistance and the number of load-bearing intact sub-cells [57]. As the thermal propagation within a cell progresses further and further, individual sub-cells begin to form short circuits and may go into thermal runaway. This leads over the propagation time to a decrease of intact sub-cells and to a change in short circuit resistance, which results in a faster voltage

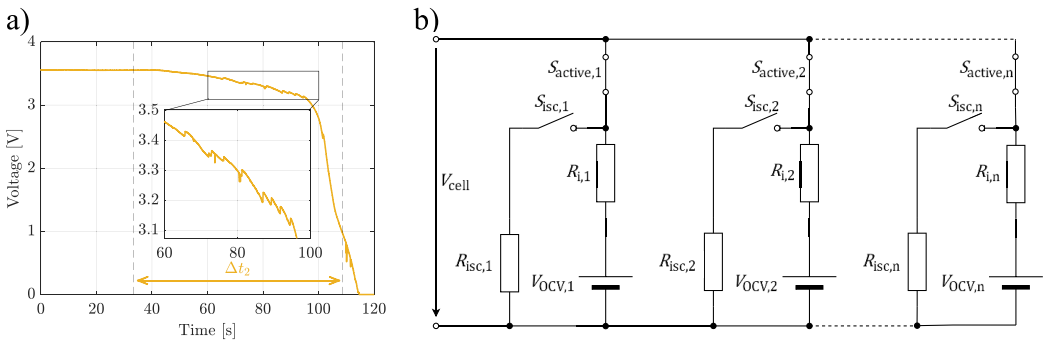


**Fig. 8.** (a) shows the zoomed plot of the voltage curve of the 20% SOC cell and (b) shows the ECM when considering a cell as a parallel connection of several sub-cells.

drop [57]. At the same time as the temperature rises on the back of the cell, this leads to a rapid acceleration of the voltage drop from approx. 95 s onwards.

The zoomed voltage curve in Fig. 8a shows a characteristic saw-tooth pattern. This suggests that at times when the voltage suddenly increases, a micro short circuit path is burnt down [59] or a sub-cell may no longer have electrical contact with the remaining sub-cells or is at least poorly electrical connected, leading to an increase of the total short circuit resistance. In terms of the ECM, this causes one of the short-circuited sub-cells in the parallel connection to fail by opening the corresponding active switch $S_{\text{active},n}$ or increasing the $R_{\text{isc}}$. This explanation of the voltage curve agrees well with the literature. Feng et al. [39] observed a five-stage voltage response of a battery consisting of two parallel pouch cells and Gao et al. [58] describe a similar behavior for the module voltage of four in parallel connected cells.

## 5. Conclusion

### 5.1. Summary

This study investigated the thermal propagation in lithium-ion battery modules with non-uniform SOC distribution. Inspired by previous studies on the SOC dependency of thermal runaway, it aimed to verify the assumption that discharging cells in the propagation path may mitigate or even stop the propagation.

Four experiments were conducted with modules consisting of three high energy 63 Ah pouch cells. The two reference experiments comprised uniform SOC distribution of all 60% and all 100%. The other two experiments comprised non-uniform SOC distribution of 100%–60%–100% and 100%–20%–100%. They represent configurations that may have been achieved by partial or progressed discharge of the middle cell through active SOC reduction techniques. The following main conclusions were drawn from the analysis of the experimental data:

- Reducing the SOC of the middle cell from 100% to 20% prolonged the total module propagation time by 87 s (factor of 2) compared to the uniform test with 100% SOC (83 s). In comparison to the less dangerous uniform test with 60% SOC (122 s), the total module propagation time was still prolonged by 48 s (factor of 1.4).
- The trigger time of a cell within the propagation path is mainly influenced by the SOC of the preceding cell and only slightly by the SOC of the considered cell itself. The higher the SOC of the considered cell or the preceding cell, the earlier the trigger time.
- A low SOC leads to a calmer thermal runaway of the considered cell, a lower maximum temperature and a prolonged propagation time within the cell and to the subsequent cell. However, the extended heating period of the subsequent cell leads to a more homogeneous temperature rise with faster internal propagation of the subsequent cell once the trigger temperature is reached.
- The tendency of the module pressure to decrease as thermal propagation progresses results in lower mass loss and slower cell internal propagation for cells with larger distance to the thermal propagation origin.
- Temperature, voltage, pressure and video data indicate that the heat and the resulting chemical reactions pass layer by layer through the cell stack. The resulting gas bubbles between the layers of the cell stack can temporarily increase the thermal resistance between the layers which slows the internal propagation.

### 5.2. Future work and limitations

While we believe that this study provides valuable insights into the SOC dependence of thermal runaway and its propagation through a module, there exist several opportunities for future research to expand and improve our understanding of this topic.

Instead of choosing SOC configurations within the cell's specification, over discharging could result in additional safety gains with respect to the mitigation of thermal propagation. In addition to the SOC, the module preload pressure seems to have a significant influence on thermal propagation, which was investigated only to a small extent in this work. A deeper understanding of this relation is required.

The results emphasize that reducing the SOC of selected cells in a module in anticipation of imminent thermal runaway may mitigate or even stop thermal propagation. This introduces new possibilities for active safety strategies in battery systems.

Implementing such a strategy requires consideration of additional factors though. Discharging a cell in the anticipation of thermal propagation generates heat, which leads to an elevated temperature when the cell is reached by the heat front of thermal propagation. This is not closely resembled in our experiments and might be a worse starting situation compared with no discharging. Furthermore, such a strategy may not be feasible in conventional battery systems, since discharging the whole battery to reduce the SOC of a few cells at sufficient rates requires an extraordinary energy sink. The strategy is also restricted to discharging all cells at the same time and at the same rate. This may be one of the first applications that draws broader attention to intelligent reconfigurable battery systems that could implement the strategy with better granularity and much lower requirements for the energy sink. After successfully applying the discharging strategy, it remains unclear whether the affected cells must be replaced immediately or may remain in the system without compromising battery safety.

## CRediT authorship contribution statement

**Michael Theiler:** Writing – review & editing, Writing – original draft, Visualization, Validation, Software, Methodology, Investigation, Formal analysis, Data curation, Conceptualization. **Alexander Baumann:** Writing – review & editing, Validation, Software, Methodology, Investigation, Formal analysis, Data curation, Conceptualization. **Christian Endisch:** Writing – review & editing, Supervision, Resources, Project administration, Funding acquisition.

## Declaration of competing interest

The authors declare that they have no known competing financial interests or personal relationships that could have appeared to influence the work reported in this paper.

## Data availability

The authors do not have permission to share data.

## Declaration of Generative AI and AI-assisted technologies in the writing process

During the preparation of this work the author(s) used ChatGPT in order to improve language and readability. After using this tool/service, the author(s) reviewed and edited the content as needed and take(s) full responsibility for the content of the publication.

## Acknowledgment

Special thanks are given to the support by Simon Diehl for revising this work and Michael Hinterberger for valuable discussions.

## Funding

This work was funded by the AUDI AG within the scope of an ongoing research project.

## References

[1] X. Feng, S. Zheng, D. Ren, X. He, L. Wang, H. Cui, X. Liu, C. Jin, F. Zhang, C. Xu, H. Hsu, S. Gao, T. Chen, Y. Li, T. Wang, H. Wang, M. Li, M. Ouyang, Investigating the thermal runaway mechanisms of lithium-ion batteries based on thermal analysis database, Appl. Energy 246 (2019) 53–64, http://dx.doi.org/10.1016/j.apenergy.2019.04.009.

[2] P. Liu, H. Sun, Y. Qiao, S. Sun, C. Wang, K. Jin, B. Mao, Q. Wang, Experimental study on the thermal runaway and fire behavior of LiNi0.8Co0.1Mn0.1O2 battery in open and confined spaces, Process Saf. Environ. Prot. 158 (2022) 711–726, http://dx.doi.org/10.1016/j.psep.2021.12.056.

[3] Cheng, Li, Ruan, Wang, Thermal runaway characteristics of a large format lithium-ion battery module, Energies 12 (16) (2019) 3099, http://dx.doi.org/10.3390/en12163099.

[4] X. Feng, L. Lu, M. Ouyang, J. Li, X. He, A 3D thermal runaway propagation model for a large format lithium ion battery module, Energy 115 (2016) 194–208, http://dx.doi.org/10.1016/j.energy.2016.08.094.

[5] C. Lee, A.O. Said, S.I. Stoliarov, Passive mitigation of thermal runaway propagation in dense 18650 lithium ion cell assemblies, J. Electrochem. Soc. 167 (9) (2020) 090524, http://dx.doi.org/10.1149/1945-7111/ab8978.

[6] X. Yang, Y. Duan, X. Feng, T. Chen, C. Xu, X. Rui, M. Ouyang, L. Lu, X. Han, D. Ren, Z. Zhang, C. Li, S. Gao, An experimental study on preventing thermal runaway propagation in lithium-ion battery module using aerogel and liquid cooling plate together, Fire Technol. 56 (6) (2020) 2579–2602, http://dx.doi.org/10.1007/s10694-020-00995-x.

[7] X. Rui, X. Feng, H. Wang, H. Yang, Y. Zhang, M. Wan, Y. Wei, M. Ouyang, Synergistic effect of insulation and liquid cooling on mitigating the thermal runaway propagation in lithium-ion battery module, Appl. Therm. Eng. 199 (2021) 117521, http://dx.doi.org/10.1016/j.applthermaleng.2021.117521.

[8] C.F. Lopez, J.A. Jeevarajan, P.P. Mukherjee, Experimental analysis of thermal runaway and propagation in lithium-ion battery modules, J. Electrochem. Soc. 162 (9) (2015) A1905–A1915, http://dx.doi.org/10.1149/2.0921509jes.

[9] D. Ouyang, J. Liu, M. Chen, J. Weng, J. Wang, An experimental study on the thermal failure propagation in lithium-ion battery pack, J. Electrochem. Soc. 165 (10) (2018) A2184–A2193, http://dx.doi.org/10.1149/2.0721810jes.

[10] J. Lamb, C.J. Orendorff, L.A.M. Steele, S.W. Spangler, Failure propagation in multi-cell lithium ion batteries, J. Power Sources 283 (2015) 517–523, http://dx.doi.org/10.1016/j.jpowsour.2014.10.081.

[11] H. Niu, C. Chen, D. Ji, L. Li, Z. Li, Y. Liu, X. Huang, Thermal-runaway propagation over a linear cylindrical battery module, Fire Technol. 56 (6) (2020) 2491–2507, http://dx.doi.org/10.1007/s10694-020-00976-0.

[12] Z. Wang, T. He, H. Bian, F. Jiang, Y. Yang, Characteristics of and factors influencing thermal runaway propagation in lithium-ion battery packs, J. Energy Storage 41 (2021) 102956, http://dx.doi.org/10.1016/j.est.2021.102956.

[13] D. Wei, M. Zhang, L. Zhu, H. Chen, W. Huang, J. Yao, Z. Yuan, C. Xu, X. Feng, Study on thermal runaway behavior of li-ion batteries using different abuse methods, Batteries 8 (11) (2022) 201, http://dx.doi.org/10.3390/batteries8110201.

[14] J. Liu, Z. Wang, J. Gong, K. Liu, H. Wang, L. Guo, Experimental study of thermal runaway process of 18650 lithium-ion battery, Materials (Basel, Switzerland) 10 (3) (2017) http://dx.doi.org/10.3390/ma10030230.

[15] O. Willstrand, M. Pushp, P. Andersson, D. Brandell, Impact of different li-ion cell test conditions on thermal runaway characteristics and gas release measurements, J. Energy Storage 68 (2023) 107785, http://dx.doi.org/10.1016/j.est.2023.107785.

[16] A.W. Golubkov, S. Scheikl, R. Planteu, G. Voitic, H. Wiltsche, C. Stangl, G. Fauler, A. Thaler, V. Hacker, Thermal runaway of commercial 18650 li-ion batteries with LFP and NCA cathodes – impact of state of charge and overcharge, RSC Adv. 5 (70) (2015) 57171–57186, http://dx.doi.org/10.1039/c5ra05897j.

[17] T. He, T. Zhang, S. Gadkari, Z. Wang, N. Mao, Q. Cai, An investigation on thermal runaway behaviour of a cylindrical lithium-ion battery under different states of charge based on thermal tests and a three-dimensional thermal runaway model, J. Clean. Prod. 388 (2023) 135980, http://dx.doi.org/10.1016/j.jclepro.2023.135980.

[18] H. Park, T. Yoon, Y. Kim, J.G. Lee, J. Kim, H.-s. Kim, J.H. Ryu, J.J. Kim, S.M. Oh, Thermal behavior of solid electrolyte interphase films deposited on graphite electrodes with different states-of-charge, J. Electrochem. Soc. 162 (6) (2015) A892–A896, http://dx.doi.org/10.1149/2.0431506jes.

[19] H. Maleki, J.N. Howard, Role of the cathode and anode in heat generation of li-ion cells as a function of state of charge, J. Power Sources 137 (1) (2004) 117–127, http://dx.doi.org/10.1016/j.jpowsour.2004.05.053.

[20] D.H. Doughty, R.E. Peter, A general discussion of li ion battery safety, Electrochem. Soc. Interface 21 (2) (2012) 37, http://dx.doi.org/10.1149/2.F03122if.

[21] C. Li, H. Wang, X. Han, Y. Wang, Y. Wang, Y. Zhang, X. Feng, M. Ouyang, An experimental study on thermal runaway behavior for high-capacity Li(Ni0.8Co0.1Mn0.1)O2 pouch cells at different state of charges, J. Electrochem. Energy Convers. Storage 18 (2) (2021) http://dx.doi.org/10.1115/1.4048936.

[22] C. Jin, Y. Sun, H. Wang, Y. Zheng, S. Wang, X. Rui, C. Xu, X. Feng, H. Wang, M. Ouyang, Heating power and heating energy effect on the thermal runaway propagation characteristics of lithium-ion battery module: Experiments and modeling, Appl. Energy 312 (2022) 118760, http://dx.doi.org/10.1016/j.apenergy.2022.118760.

[23] H. Li, Q. Duan, C. Zhao, Z. Huang, Q. Wang, Experimental investigation on the thermal runaway and its propagation in the large format battery module with Li(Ni1/3Co1/3Mn1/3)O2 as cathode, J. Hazard. Mater. 375 (2019) 241–254, http://dx.doi.org/10.1016/j.jhazmat.2019.03.116.

[24] Y. Liu, H. Niu, J. Liu, X. Huang, Layer-to-layer thermal runaway propagation of open-circuit cylindrical li-ion batteries: Effect of ambient pressure, J. Energy Storage 55 (2022) 105709, http://dx.doi.org/10.1016/j.est.2022.105709.

[25] J. Fang, J. Cai, X. He, Experimental study on the vertical thermal runaway propagation in cylindrical lithium-ion batteries: Effects of spacing and state of charge, Appl. Therm. Eng. 197 (2021) 117399, http://dx.doi.org/10.1016/j.applthermaleng.2021.117399.

[26] M. Zhu, S. Zhang, Y. Chen, L. Zhao, M. Chen, Experimental and analytical investigation on the thermal runaway propagation characteristics of lithium-ion battery module with NCM pouch cells under various state of charge and spacing, J. Energy Storage 72 (2023) 108380, http://dx.doi.org/10.1016/j.est.2023.108380.

[27] W. Wu, Q. Ke, J. Guo, Y. Wang, Y. Qiu, J. Cen, F. Jiang, Experimental investigation of thermal runaway propagation in a lithium-ion battery pack: Effects of state of charge and coolant flow rate, Batteries 9 (11) (2023) 552, http://dx.doi.org/10.3390/batteries9110552.

[28] T. Ying, S. Yang, W. Jiafeng, C. Mu, H. Liansheng, Thermal runaway propagation characteristics of lithium-ion batteries with a non-uniform state of charge distribution, J. Solid State Electrochem. 27 (8) (2023) 2185–2197, http://dx.doi.org/10.1007/s10008-023-05496-9.

[29] X. Hu, K. Zhang, K. Liu, X. Lin, S. Dey, S. Onori, Advanced fault diagnosis for lithium-ion battery systems: A review of fault mechanisms, fault features, and diagnosis procedures, IEEE Ind. Electron. Mag. 14 (3) (2020) 65–91, http://dx.doi.org/10.1109/MIE.2020.2964814.

[30] S. Yin, J. Liu, B. Cong, Review of thermal runaway monitoring, warning and protection technologies for lithium-ion batteries, Processes 11 (8) (2023) 2345, http://dx.doi.org/10.3390/pr11082345.

[31] X. Zhang, S. Chen, J. Zhu, Y. Gao, A critical review of thermal runaway prediction and early-warning methods for lithium-ion batteries, Energy Mater. Adv. 4 (2023) http://dx.doi.org/10.34133/energymatadv.0008.

[32] X. Feng, D. Ren, X. He, M. Ouyang, Mitigating thermal runaway of lithium-ion batteries, Joule 4 (4) (2020) 743–770, http://dx.doi.org/10.1016/j.joule.2020.02.010.

[33] J. Zhang, L. Zhang, F. Sun, Z. Wang, An overview on thermal safety issues of lithium-ion batteries for electric vehicle application, IEEE Access 6 (2018) 23848–23863, http://dx.doi.org/10.1109/ACCESS.2018.2824838.

[34] X. Hu, F. Gao, Y. Xiao, D. Wang, Z. Gao, Z. Huang, S. Ren, N. Jiang, S. Wu, Advancements in the safety of lithium-ion battery: The trigger, consequence and mitigation method of thermal runaway, Chem. Eng. J. 481 (2024) 148450, http://dx.doi.org/10.1016/j.cej.2023.148450.

[35] L. Komsiyska, T. Buchberger, S. Diehl, M. Ehrensberger, C. Hanzl, C. Hartmann, M. Hölzle, J. Kleiner, M. Lewerenz, B. Liebhart, M. Schmid, D. Schneider, S. Speer, J. Stöttner, C. Terbrack, M. Hinterberger, C. Endisch, Critical review of intelligent battery systems: Challenges, implementation, and potential for electric vehicles, Energies 14 (18) (2021) 5989, http://dx.doi.org/10.3390/en14185989.

[36] X. Feng, X. He, M. Ouyang, L. Lu, P. Wu, C. Kulp, S. Prasser, Thermal runaway propagation model for designing a safer battery pack with 25 Ah LiNi Co Mn O2 large format lithium ion battery, Appl. Energy 154 (2015) 74–91, http://dx.doi.org/10.1016/j.apenergy.2015.04.118.

[37] W. Luo, S. Cheng, M. Wu, X. Zhang, D. Yang, X. Rui, A review of advanced separators for rechargeable batteries, J. Power Sources 509 (2021) 230372, http://dx.doi.org/10.1016/j.jpowsour.2021.230372.

[38] P.V. Chombo, Y. Laoonual, Prediction of the onset of thermal runaway and its thermal hazards in 18650 lithium-ion battery abused by external heating, Fire Saf. J. 129 (2022) 103560, http://dx.doi.org/10.1016/j.firesaf.2022.103560.

[39] X. Feng, J. Sun, M. Ouyang, F. Wang, X. He, L. Lu, H. Peng, Characterization of penetration induced thermal runaway propagation process within a large format lithium ion battery module, J. Power Sources 275 (2015) 261–273, http://dx.doi.org/10.1016/j.jpowsour.2014.11.017.

[40] T. Deich, M. Storch, K. Steiner, A. Bund, Effects of module stiffness and initial compression on lithium-ion cell aging, J. Power Sources 506 (2021) 230163, http://dx.doi.org/10.1016/j.jpowsour.2021.230163.

[41] D.P. Finegan, M. Scheel, J.B. Robinson, B. Tjaden, I. Hunt, T.J. Mason, J. Millichamp, M. Di Michiel, G.J. Offer, G. Hinds, D.J.L. Brett, P.R. Shearing, In-operando high-speed tomography of lithium-ion batteries during thermal runaway, Nature Commun. 6 (2015) 6924, http://dx.doi.org/10.1038/ncomms7924.

[42] S. Hoelle, S. Zimmermann, O. Hinrichsen, 3D thermal simulation of thermal runaway propagation in lithium-ion battery cell stack: Review and comparison of modeling approaches, J. Electrochem. Soc. 170 (6) (2023) 060516, http://dx.doi.org/10.1149/1945-7111/acd966.

[43] Z. Huang, X. Li, Q. Wang, Q. Duan, Y. Li, L. Li, Q. Wang, Experimental investigation on thermal runaway propagation of large format lithium ion battery modules with two cathodes, Int. J. Heat Mass Transfer 172 (2021) 121077, http://dx.doi.org/10.1016/j.ijheatmasstransfer.2021.121077.

[44] K. Li, J. Li, X. Gao, Y. Lu, D. Wang, W. Zhang, W. Wu, X. Han, Y.-c. Cao, L. Lu, J. Wen, S. Cheng, M. Ouyang, Effect of preload forces on multidimensional signal dynamic behaviours for battery early safety warning, J. Energy Chem. 92 (2024) 484–498, http://dx.doi.org/10.1016/j.jechem.2023.12.045.

[45] M. Steinhardt, E.I. Gillich, M. Stiegler, A. Jossen, Thermal conductivity inside prismatic lithium-ion cells with dependencies on temperature and external compression pressure, J. Energy Storage 32 (2020) 101680, http://dx.doi.org/10.1016/j.est.2020.101680.

[46] L. Tendera, D. Wycisk, C. Gonzalez, G.K. Mertin, H. Pegel, K.P. Birke, Effects of geometric, structural and operational parameters on the thermal conductivity of lithium-ion cells, J. Power Sources 549 (2022) 232120, http://dx.doi.org/10.1016/j.jpowsour.2022.232120.

[47] Z. Mao, M. Farkhondeh, M. Pritzker, M. Fowler, Z. Chen, Calendar aging and gas generation in commercial graphite/NMC-LMO lithium-ion pouch cell, J. Electrochem. Soc. 164 (14) (2017) A3469–A3483, http://dx.doi.org/10.1149/2.0241714jes.

[48] V. Müller, R.-G. Scurtu, K. Richter, T. Waldmann, M. Memm, M.A. Danzer, M. Wohlfahrt-Mehrens, Effects of mechanical compression on the aging and the expansion behavior of Si/C-composite|NMC811 in different lithium-ion battery cell formats, J. Electrochem. Soc. 166 (15) (2019) A3796–A3805, http://dx.doi.org/10.1149/2.1121915jes.

[49] X. Feng, F. Zhang, W. Huang, Y. Peng, C. Xu, M. Ouyang, Mechanism of internal thermal runaway propagation in blade batteries, J. Energy Chem. 89 (2024) 184–194, http://dx.doi.org/10.1016/j.jechem.2023.09.050.

[50] J. Chen, D. Ren, H. Hsu, L. Wang, X. He, C. Zhang, X. Feng, M. Ouyang, Investigating the thermal runaway features of lithium-ion batteries using a thermal resistance network model, Appl. Energy 295 (2021) 117038, http://dx.doi.org/10.1016/j.apenergy.2021.117038.

[51] Z. Huang, T. Shen, K. Jin, J. Sun, Q. Wang, Heating power effect on the thermal runaway characteristics of large-format lithium ion battery with Li(Ni1/3Co1/3Mn1/3)O2 as cathode, Energy 239 (2022) 121885, http://dx.doi.org/10.1016/j.energy.2021.121885.

[52] A. Hahn, S. Doose, D. Saathoff, A. Kwade, Effect of external compression on the thermal runaway of lithium-ion battery cells during crush tests: Insights for improved safety assessment, Batteries 9 (8) (2023) 404, http://dx.doi.org/10.3390/batteries9080404.

[53] Y. Li, X. Liu, L. Wang, X. Feng, D. Ren, Y. Wu, G. Xu, L. Lu, J. Hou, W. Zhang, Y. Wang, W. Xu, Y. Ren, Z. Wang, J. Huang, X. Meng, X. Han, H. Wang, X. He, Z. Chen, K. Amine, M. Ouyang, Thermal runaway mechanism of lithium-ion battery with LiNi0.8Mn0.1Co0.1O2 cathode materials, Nano Energy 85 (2021) 105878, http://dx.doi.org/10.1016/j.nanoen.2021.105878.

[54] Y. Zhao, Y. Patel, T. Zhang, G.J. Offer, Modeling the effects of thermal gradients induced by tab and surface cooling on lithium ion cell performance, J. Electrochem. Soc. 165 (13) (2018) A3169–A3178, http://dx.doi.org/10.1149/2.0901813jes.

[55] Y. Xie, W. Li, X. Hu, C. Zou, F. Feng, X. Tang, Novel mesoscale electrothermal modeling for lithium-ion batteries, IEEE Trans. Power Electron. 35 (3) (2020) 2595–2614, http://dx.doi.org/10.1109/TPEL.2019.2927014.

[56] M. Ouyang, M. Zhang, X. Feng, L. Lu, J. Li, X. He, Y. Zheng, Internal short circuit detection for battery pack using equivalent parameter and consistency method, J. Power Sources 294 (2015) 272–283, http://dx.doi.org/10.1016/j.jpowsour.2015.06.087.

[57] M. Chen, S. Lin, W. Song, J. Lv, Z. Feng, Electrical and thermal interplay in lithium–ion battery internal short circuit and safety protection, Int. J. Energy Res. 44 (8) (2020) 6745–6757, http://dx.doi.org/10.1002/er.5411.

[58] S. Gao, X. Feng, L. Lu, N. Kamyab, J. Du, P. Coman, R.E. White, M. Ouyang, An experimental and analytical study of thermal runaway propagation in a large format lithium ion battery module with NCM pouch-cells in parallel, Int. J. Heat Mass Transfer 135 (2019) 93–103, http://dx.doi.org/10.1016/j.ijheatmasstransfer.2019.01.125.

[59] M. Zhang, L. Liu, A. Stefanopoulou, J. Siegel, L. Lu, X. He, M. Ouyang, Fusing phenomenon of lithium-ion battery internal short circuit, J. Electrochem. Soc. 164 (12) (2017) A2738–A2745, http://dx.doi.org/10.1149/2.1721712jes.